We are IntechOpen, the world's leading publisher of Open Access books Built by scientists, for scientists

4,800
Open access books available

122,000
International authors and editors

135M
Downloads

Our authors are among the

154
Countries delivered to

TOP 1%
most cited scientists

12.2%
Contributors from top 500 universities

CLARIVATE ANALYTICS BOOK CITATION INDEX INDEXED

WEB OF SCIENCE™

Selection of our books indexed in the Book Citation Index in Web of Science™ Core Collection (BKCI)

Interested in publishing with us?
Contact book.department@intechopen.com

Numbers displayed above are based on latest data collected.
For more information visit www.intechopen.com

3

Unambiguous Processing Techniques of Binary Offset Carrier Modulated Signals

Zheng Yao
Tsinghua University
China

1. Introduction

In recent years, applications of global navigation satellite systems (GNSS) are developing rapidly. The growing public demand for positioning and location services has generated higher requirements for system performance. However, the performance of the traditional GPS is constrained by its inherent capability. In order to cope with both the civil and military expectations in terms of performance, several projects are launched to promote the next generation of GNSS (Hegarty & Chatre, 2008). GPS is undergoing an extensive modernization process (Enge, 2003), while the European satellite system, Galileo, is also under construction. In addition, Russia is restoring their GLONASS (Slater et al., 2004), and China is in the midst of launching Compass (Gao et al., 2007).

Based on the experience gained during the traditional GPS design and operation, signal structures of these new navigation systems have been well designed (ARINC, 2005, 2006). A large number of modifications have been made intended to address the main weakness of traditional GPS, and to enhance its inherent performance. The accuracy and reliability of those modernized signals and the compatibility between new signals and already-existing signals have been simultaneously taken into account in the design.

Binary offset carrier (BOC) (Betz, 2001) and multiplexed binary offset carrier (MBOC) modulations (Hein et al., 2006) have been chosen as the chief candidate for several future navigation signals, for example, GPS L1C, GPS M-code, and Galileo open service (OS) signals. BOC modulation is a square-wave modulation scheme. It moves signal energy away from the band center and thus achieves a higher degree of spectral separation between BOC modulated signals and other signals which use traditional binary phase shift keying (BPSK) modulation, such as the GPS C/A code, in order to get a more efficient sharing of the L-band spectrum. Besides, many studies (Avila-Rodriguez, et al., 2007; Betz, 2001; Hein, et al., 2006) show that BOC modulation also provides better inherent resistance to multipath and narrowband interference.

However, despite these advantages, some problems remain with the use of BOC modulation. According to the theory of matched filtering (Proakis, 2001), when the waveform of the local signal is as same as the received one, the output of the correlator has the highest signal-noise-ratio (SNR). For this reason, in traditional GPS receivers, both of the acquisition and tracking are based upon the auto-correlation function (ACF) of the received

signals. Nevertheless, because of the square-wave modulated symbol, a BOC modulated signal has a sawtooth-like, piecewise linear ACF which has multiple non-negligible side peaks along with the main peak. Since there are significant amount of signal energy located at side peaks of BOC ACF, in acquisition stage, under the influence of noise it is quite likely that one of side peak magnitudes exceeds the main peak, and false acquisition will happen. If false acquisition occurs, the code tracking loop will initially lock on the side peak. Similarly, due to the side peaks of ACF, in code tracking loop, the discriminator characteristic curve of a BOC modulated signal has multiple stable false lock points. Once the loop locks on one of the side peaks, it would result in intolerable bias in pseudorange measurements, which is unacceptable for GNSS aiming to provide accurate navigation solution. This problem is reputed as the ambiguity problem for BOC modulated signal acquisition and tracking. And in order to employ BOC modulated signals in the next generation GNSS, solutions have to be found to minimize this bias threat.

In this Chapter, the ambiguity problem of BOC modulated signals as well as its typical solutions is systematically described. An innovative design methodology for future unambiguous processing techniques is also proposed. Some practical design examples on this methodology are also given to show the practicality and to provide reference to further algorithm development.

The rest of the Chapter is organized as follows. In Section 2, the concept and some main characteristics of BOC modulated signals are given, and the ambiguity problem is also described. In Section 3, some existing representative solutions to ambiguity problem are reviewed. Then in Section 4, we present a parameterized chip waveform pattern, and on this basis, give the analytic design framework for side-peak cancellation (SC) based unambiguous BOC signal processing algorithm development. As two application examples of the proposed design framework, the design process of an SC unambiguous acquisition algorithm as well as an SC unambiguous tracking loop is described in Section 5 and Section 6, respectively. Finally, some conclusions are drawn in Section 7.

2. BOC modulated signals

2.1 Definitions and main characteristics

In order to take advantage of the frequent phase inversions in the spreading waveform to realize the precise ranging, and to obtain excellent multiple access capability, the majority of GNSS employ direct sequence spread spectrum (DSSS) technique. DSSS can be regarded as an extension of binary phase shift keying (BPSK). The transmitting signal yielded by this technique can be expressed as the product of the un-modulated carrier, data $d(t)$, as well as the baseband spreading signal $g(t)$, that is

$$s(t) = A_s d(t) g(t) \cos(2\pi f_0 t + \theta) \tag{1}$$

where A_s is the amplitude of signal, f_0 is the carrier frequency in Hz, and θ is the carrier phase in radians. The baseband spreading signal $g(t)$ can be further represented as

$$g(t) = \sum_{i=-\infty}^{\infty} (-1)^{c_i} p(t - iT_c) \tag{2}$$

where c_i is the spreading sequence of binary digits {0,1}, $p(t)$ is spreading symbol, and T_c is the period of the modulated symbol. In conventional GPS, both of C/A code signal and P(Y) code signal use BPSK-R(n) modulation whose spreading symbol is the energy normalized rectangular pulse with the lasting time $T_c = 1/(n \times 1.023\text{MHz})$:

$$p_{\text{BPSK-R}}(t) = \begin{cases} \dfrac{1}{\sqrt{T_c}}, & 0 \le t < T_c \\ 0, & \text{others} \end{cases} \tag{3}$$

In principle, the spreading symbol of DSSS signals can be any shape. BOC modulated signal is a variant of basic DSSS signal. The baseband BOC modulated signal can be regarded as the result of multiplying the BPSK-R signal with a sub-carrier which is equal to the sign of a sine or a cosine waveform:

$$s_{\text{BOC}}(t) = s_{\text{BPSK-R}}(t)\,\text{sgn}\left[\sin\left(2\pi f_s t + \phi\right)\right] \tag{4}$$

where $\text{sgn}(\cdot)$ is sign function, f_s is the sub-carrier frequency, and ϕ is the phase of sub-carrier. Two common values of ϕ are 0 or $\pi/2$, for which the resultant BOC signals are referred to as sine-phased BOC or cosine-phased BOC, respectively. In this Chapter, we focus on sine-phased case. For information on cosine-phased BOC signal unambiguous processing, see (Lohan et al., 2008). Using the terminology from (Betz, 2001), a sine phased BOC modulated signal is denoted as BOC$_s$(m,n), where m means the ratio of the square wave frequency f_s to 1.023 MHz, and n represents the ratio of the spreading code rate f_c to 1.023 MHz. m and n are constrained to positive integer $m \ge n$, and the ratio $M = 2m/n$ is referred to as BOC-modulation order, which is constrained to positive integer.

Under the assumption that the spreading sequence has an ideal correlation characteristic, the power spectrum density (PSD) of $\text{BOC}_s(f_s, f_c)$ can be expressed as (Betz, 2001)

$$S_{\text{BOC}_s}(f) = \begin{cases} T_c \dfrac{\sin^2(\pi f T_c)}{(\pi f T_c)^2} \tan^2\left(\dfrac{\pi f}{2 f_s}\right), & M \text{ even} \\ T_c \dfrac{\cos^2(\pi f T_c)}{(\pi f T_c)^2} \tan^2\left(\dfrac{\pi f}{2 f_s}\right), & M \text{ odd} \end{cases} \tag{5}$$

It can be seen that due to the effect of subcarrier, BOC modulated signals symmetrically split the main energy component of the signal spectrum and move them away from the band center, so that they have a higher degree of spectral separation with other BPSK-R modulated signals on the same carrier frequency. Moreover, as noted in (Betz, 2001), BOC modulated signals have greater root-mean-square (RMS) bandwidth compared with traditional BPSK signals with the same spreading code frequency. The greater the RMS bandwidth is, the better the inherent ability to mitigate white Gaussian noise and narrowband interference during tracking will be. Consequently, with same f_c, BOC modulation provides better resistance to thermal noise and narrowband interference than BPSK-R modulation theoretically. However, the ambiguity of the autocorrelation function of sine-BOC modulated signal induces a risk of biased measures in code synchronization.

2.2 Ambiguous problem

The difference of the spreading chip waveforms between BPSK-R signals and BOC signals leads their difference in ACF shapes, and thus makes the distinction of acquisition and tracking performance. The ACF of BPSK-R modulated signals is a triangle, but BOC signals have sawtooth-like, piecewise linear ACF. The normalized BOC(*m*,*n*) ACF without filter can be expressed as (Yao, 2009)

$$R_{\mathrm{BOC}}(\tau)=\begin{cases}(-1)^{k+1}\left[\left(-\dfrac{2k^2-2k}{M}+2k-1\right)-(2M-2k+1)|\tau|\right], & |\tau|\le T_c\\ 0, & \text{others}\end{cases} \tag{6}$$

where $k=\lceil M\cdot|\tau|\rceil$, and $\lceil x\rceil$ means the smallest integer not less than x. In Figure 1, the normalized ACF envelopes of BPSK-R(1) signal and BOC(2,1) signal are drawn.

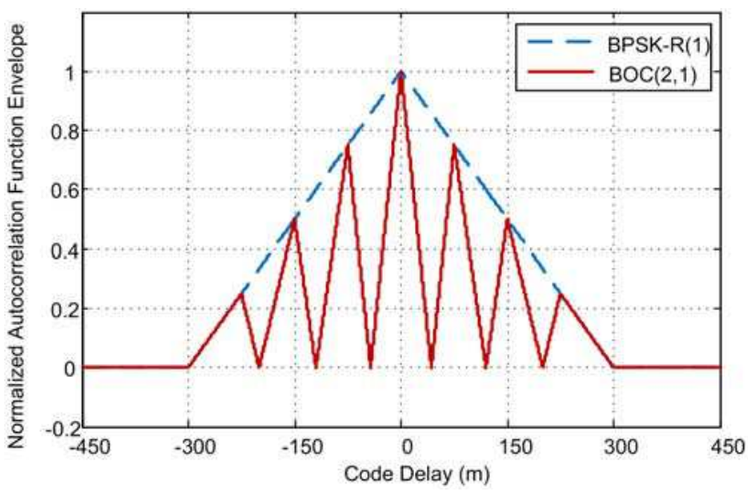

Fig. 1. BPSK-R(1) and BOC(2,1) Normalized ACF Envelopes

From Figure 1 we can see that these two signals have the same spreading chip rate 1.023 MHz, but their ACFs have entirely different shapes. Compared with the triangular ACF of BPSK-R(1) signal, that of BOC(2,1) signal has a sharper main peak, which means better tracking accuracy in thermal noise. However, the ACF of BOC signal has multiple side peaks within $\tau=\pm1$ chips. At the acquisition and tracking stages, these side peaks could be mistaken for the main peak.

When the traditional acquisition and tracking algorithms are employed to process BOC(2*n*,*n*) signal, the shapes of statistic and the discriminator curve are shown in Figure 2(a) and Figure 2(b), respectively.

The traditional acquisition and tracking of DSSS signal have been very well discussed (Ziemer & Peterson, 1985). From Figure 2(a) we can see that since there are significant amount of signal energy located at side peaks of BOC ACF, under the influence of noise it is quite likely that one of side peak magnitudes exceeds the main peak, and false acquisition will happen. For *M*-order BOC signal, the energy ratio between the *i*-th largest side peak and the main peak is

$$\xi_i = \left(\frac{M-i}{M} \right)^2 \tag{7}$$

For $M = 2$, side peaks are 6 dB weaker than the main peak. But for $M = 6$, the gap between the largest side peak and the main peak is only 2.5 dB. With increase of M, the difference between the maximum side peak and the main peak decreases, while the false acquisition probability increase.

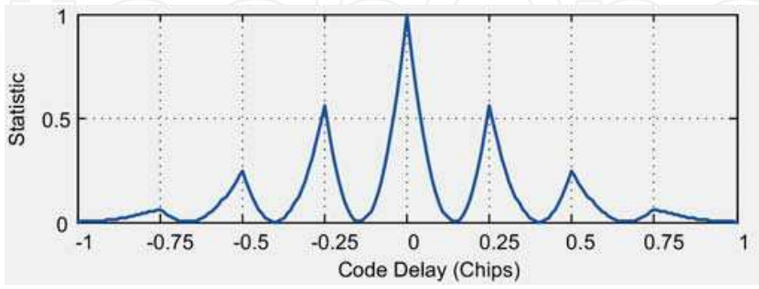

(a)

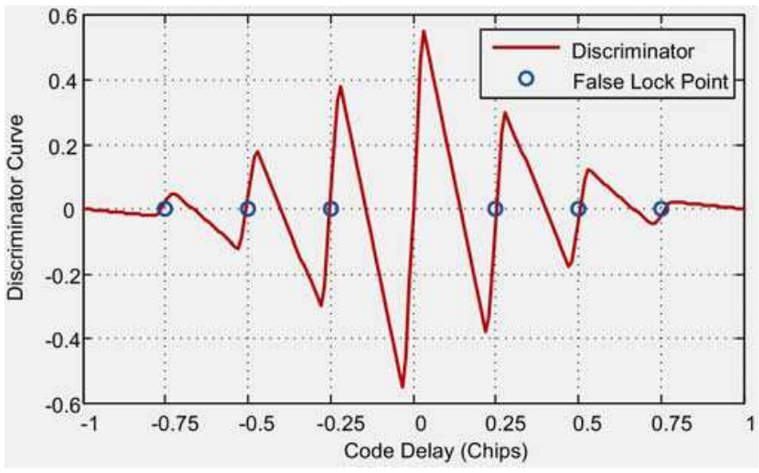

(b)

Fig. 2. (a) The Statistic in Acquisition Stage and (b) The Discriminator Curve in Tracking Stage of BOC(2*n*,*n*) Signal

It can be seen from Figure 2(b) that when using a traditional narrow early-minus-late (NEML) tracking loop (Van Dierendonck et al., 1992) with the early-late separation Δ, the discriminator characteristic curve of BOC(*m*,*n*) signal has a smaller linear domain than the one of the BPSK-R(*n*) signal. Besides, the discriminator characteristic curve of a BOC(*m*,*n*) signal has $2M - 2$ stable false lock points which are due to the side peaks of the autocorrelation function. If a false acquisition occurs, in tracking stage, the code tracking loop will initially lock on a false lock point. Even if there is no false acquisition, the false lock can result from high noise, jitter, or short loss of lock.

Figure 3 shows an example of false lock caused by the excessive initial code delay bias in BOC(2*n*,*n*) signal tracking. The C/N_0 in this example is 45 dB-Hz, and the predetection integration time is 1 ms, with the early-late separation 0.1 chips. It can be seen that with the

initial code delay bias of 0.14 chips, the loop locks on a false lock point. Although the output of discriminator hovers around zero and DLL maintains lock, the true code phase measurement bias is 0.25 chips, which corresponds to 75 m for BOC(2,1) signal. Such a considerable bias is unacceptable in most of the positioning applications.

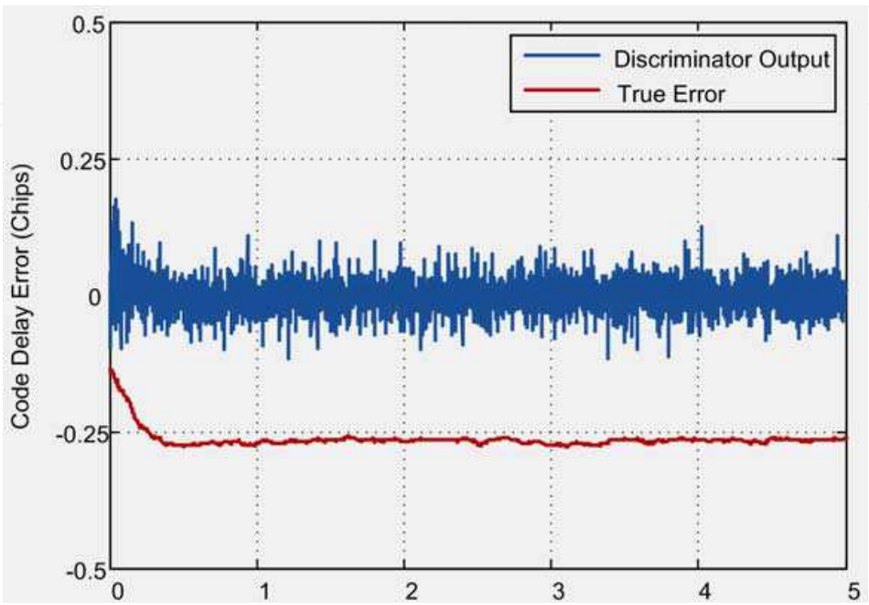

Fig. 3. Example of False Lock in Traditional DLL

3. Existing unambiguous processing techniques

During the decade from when BOC modulation was initially proposed to the present time, several solutions have been proposed to solve the ambiguity problem. In summary, the elimination of ambiguity threat can be achieved via two ways: false lock detection and recovery technique, as well as unambiguous processing techniques. More specifically, considering the operation domain, unambiguous processing can be further classified into frequency-domain processing and time-domain processing.

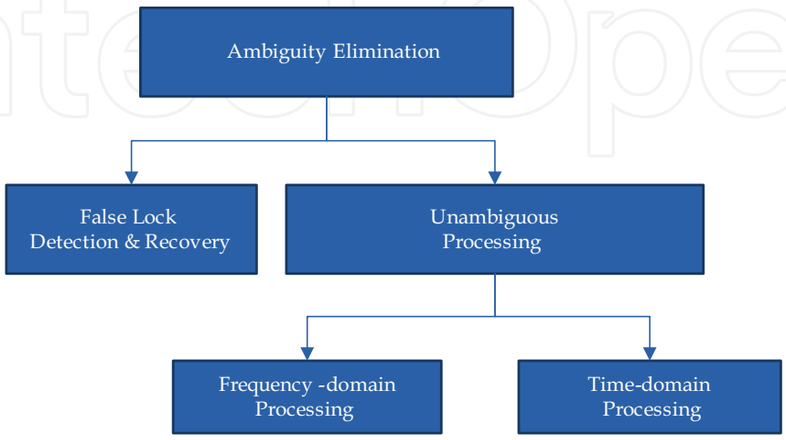

Fig. 4. Existing Ambiguity Elimination Solutions

3.1 False lock detection & recovery

False lock detection and recovery technique does not remove ambiguity but rather checks false lock. The most representative detection and recovery technique is referred to as bump-jumping technique (Fine & Wilson, 1999). This technique employs the traditional ambiguous code tracking loop and constantly check whether this loop is locked on the main peak of BOC ACF. To do so, bump-jumping technique uses two additional correlators located at the theoretical location of the two highest side peaks, as shown in Figure 5.

These two correlators are referred to as very early (VE) and very late (VL) correlators. By measuring and comparing the magnitude of the outputs of these two correlators and the prompt one, bump-jumping technique determines whether the false lock happens. It can be seen from Figure 5 that ignoring the effect of noise, when the code loop locks on the main peak, the magnitude of prompt correlator output is the greatest. And if either VE or VL correlator output is the largest, it means that tracking might be biased, and the loop will "jump" in the appropriate direction.

When locked on the main peak, this technique has high tracking accuracy. However, since it is based on the comparing of the main and side peaks magnitudes, the detection may have a high probability of false alarm when the signal-to-noise ratio (SNR) is low. In (Fine & Wilson, 1999), two up/down counter mechanisms are employed to reduce this false alarm probability. After each comparison, if one of the magnitudes of VE and VL correlator outputs exceeds that of the prompt one, the corresponding counter is incremented by one, otherwise the corresponding counter is decremented by one. The counter is not decremented below 0 or incremented above the preset threshold N. When the counter reaches the threshold, the loop jumps to the highest peak. By using this counter mechanism, the false alarm probability can be reduced effectively. However, the response time is also increased. Once the false lock happen, this technique needs time to detect and recover from false lock, so it might be intolerable for some critical applications such as aircraft landing.

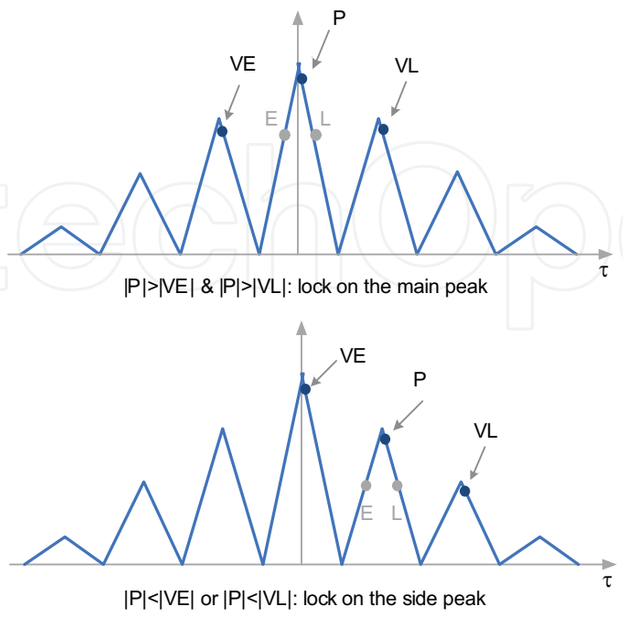

Fig. 5. Bump-jumping technique

3.2 Frequency-domain unambiguous processing

Frequency-domain processing techniques are represented by sideband techniques. Sideband technique considers the received BOC signal as the sum of two BPSK signals with carrier frequency symmetrically positioned on each side of the BOC carrier frequency. Thus each side lobe is treated independently as a BPSK signal, which provides an unambiguous correlation function and a wider S-curve steady domain.

The earliest sideband technique was described in (Fishman & Betz, 2000). As shown in Figure 6, the single sideband technique uses only one of the sidebands (either upper or lower) of BOC modulated signal. Both the received signal and the local BOC modulated baseband signal are filtered. Only the upper or lower sidebands of the received and local signals are retained. The shape of the correlation function of these two filtered signals is close to that of two BPSK-R signals. Therefore this correlation function can be used instead of BOC ACF in acquisition and tracking. The double sideband technique uses both the upper and lower sideband of BOC modulated signal. These two sidebands are processed separately before the output of correlators, and then the correlation values are added non-coherently. Compared with single sideband technique, double sideband technique suffers lower non-coherent correlation losses. However, it requires twice the sideband-selection filter number of single sideband technique.

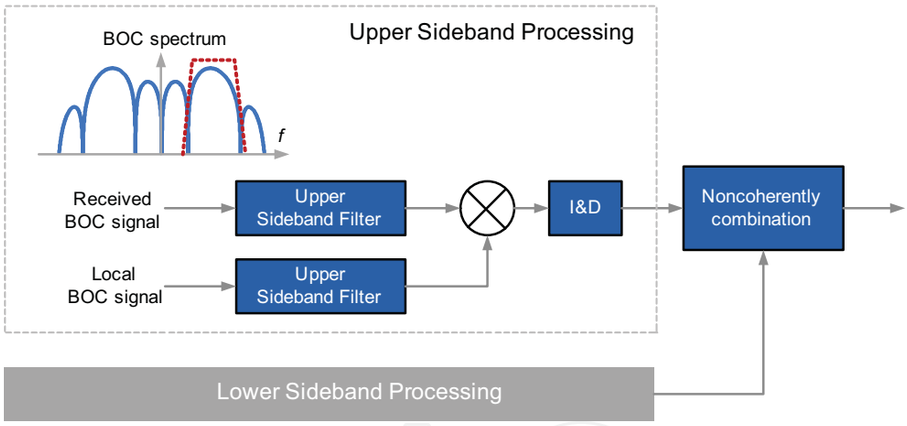

Fig. 6. Block diagram of sideband technique

BPSK-like method (Martin et al., 2003) is another frequency-domain unambiguous processing technique. This method is also based on the consideration of the BOC spectrum as the sum of two BPSK spectrum shifted by $\pm f_s$. The main difference compared with the method described above is the fact that only one low-pass filter is employed for the received signal. As shown in Figure 7, the filter bandwidth includes the two principal lobes of the spectrum. Another difference is that, the local signal is not the filtered BOC-modulated baseband signal but the BPSK-R signal, shifted by the sub-carrier frequency f_s. The BPSK-like technique can also be either single or double sideband, according to whether both the sidebands are used and combined non-coherently or only one sideband is used.

The original BPSK-like method can only be used for sine-phased BOC modulations with even BOC order. In (Burian et al., 2006), a modified version of BPSK-like method is proposed to extend BPSK-like method to BOC signals with odd order.

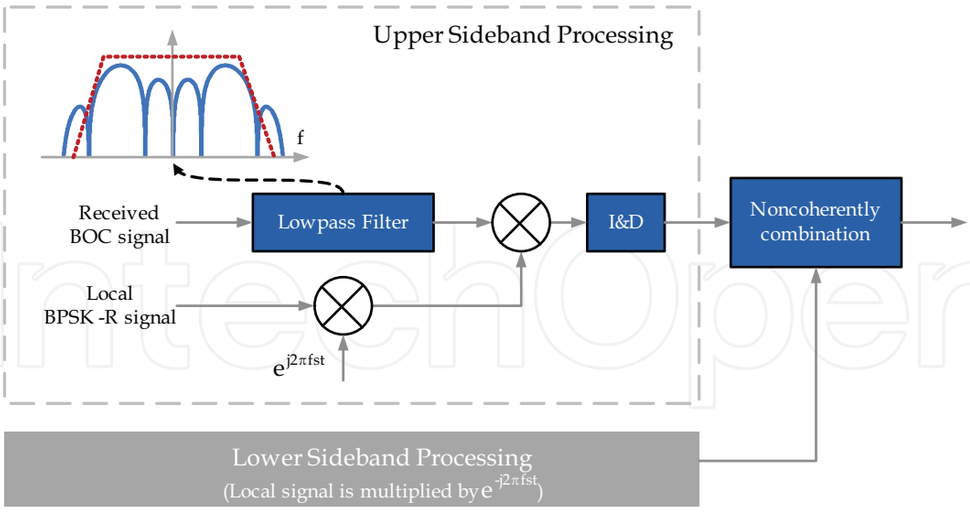

Fig. 7. Block diagram of BPSK-like method

Although the correlation functions in sideband techniques do not present any side peak, meaning that they are fully unambiguous, this kind of methods suffers from some drawbacks. The principle defect is that this kind of methods completely removes all of the advantages of BOC signal tracking in terms of Gaussian noise and multipath mitigation, since it causes the Gabor bandwidth of the received signal to approach that of the BPSK-R signal. Moreover, two side lobes are combined in non-coherent mode, which introduces correlation losses into the process. It seems that sideband techniques are not appropriate in terms of tracking. However, the correlation functions in this kind of methods have wide main correlation peak, which allows using longer code delay step in acquisition to reduce mean acquisition time. Therefore, sideband techniques can be attractive options in BOC modulated signal acquisition.

3.3 Time-domain unambiguous processing

Time-domain processing techniques are also referred to as side-peaks cancellation (SC) techniques which solve the ambiguity problem by taking advantage of the geometrical property of correlation functions (CF). The basic idea of SC techniques is using synthesized correlation function (SCF) instead of BOC ACF in acquisition and tracking. CF between the received BOC signal and some local auxiliary signals whose chip waveforms may be different from the received one are combined linearly or non-linearly to form the SCF with no side-peak. SC methods are flexible. Due to different auxiliary signal chip waveforms and combination modes, SC methods differentiate from each other greatly.

The first side-peaks cancellation technique is proposed in (Ward, 2003). This approach removes the ambiguities of the correlation function, but one drawback is that this method destroys the sharp peak of the correlation function. For accurate tracking, preserving a sharp peak of the correlation function is a prerequisite. An innovative unambiguous tracking technique, which is referred to as autocorrelation side-peak cancellation technique (ASPeCT), is described in (Julien et al., 2007). This technique uses ten correlation channels, completely removing the side peaks from the correlation function and keeping the sharp

main peak. However, this technique has some limitations, for it is only applicable to sine-BOC(n,n) signals. Some other side-peaks cancellation methods have been proposed recently (Dovis, et al., 2005; Fante, 2003; Musso et al., 2006; Nunes et al., 2007).

However, the design of SC algorithms is still scarce of uniform theoretical frame and analytical method. There is no easy handling design method for SC algorithms development. The key of SC methods is the selection of local auxiliary signal chip waveforms. Due to lack of mathematical analysis tools, the selection of local signal chip waveforms is mainly based on intuition and trail-and-error. In new SC algorithm design, the shape of auxiliary signal waveforms is limited by the imagination of the designer, thus concentrating on some common shapes such as rectangular pulse, square wave with sine phase or cosine phase, and return to zero (RZ) code wave. When the chip waveform of the received signal is simple, for instance, Manchester code which is used in BOC(n,n) signals, it is easy to find a corresponding auxiliary chip waveform by using trail-and-error method. However, when the chip waveform of target signal gets more complicated, the design process becomes tough, and a mathematical analysis method is needed.

In the next section, a SC analytic design framework is presented. In this framework, the local auxiliary signal chip waveform can be designed under this framework by means of mathematic analysis so that the waveform shape selection can be more flexible.

4. SC analytic design framework

4.1 SCS waveform

The main difficulty of SC method design is how to select the spreading code chip waveform of local signals. It is desired to define a parameterized local signal model the chip waveform of which has a high degrees of freedom and is easy to generate in receivers to provide more opportunities for waveform optimization. Although there are few investigations about general local signal model for receiver designers since most of the signal receiving techniques are based on matched correlator in GNSS, it is interesting to note that some generalized waveform models are proposed for satellite signal design in order to offer degrees of freedom for shaping the signal spectrum, such as the binary coded symbols (BCS) (Hegarty et al., 2004). The advanced idea can be instructive for SC algorithm design.

For BCS signals, in order to ensure constant modulus, the envelope of $p(t)$ is restricted to 1. However, when considering auxiliary chip waveform in SC techniques, since local signals do not relate to amplifying and transmitting, they do not need to satisfy the request of constant modulus but their chip waveform should be easy to generate. Therefore, we expand the definition of BCS signal, restricting the chip waveform to being real-valued and having normalized energy. The chip waveform is divided into M segments, each with equal length $T_s = T_c / M$, and in each segment the level remains constant.

Since such waveform looks like steps, for expressional simplicity, we call this kind of chip waveform the step-shape code symbol (SCS) waveform, and call the signal which uses this waveform the SCS signal hereafter. Sticking with the terms used for BOC signals, M is referred to as the order of SCS signal. Some examples of SCS waveforms are shown in Figure 8.

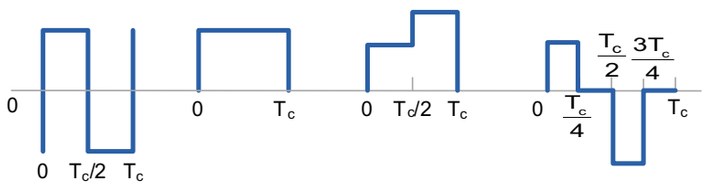

Fig. 8. Examples of SCS Waveforms

4.2 Vector representation

Any SCS waveform can be represented by a coordinate vector. Given a pair of T_c and T_s, we can construct a set of function $\{\psi_k(t): k=0,1,\cdots,M-1\}$, where

$$\psi_k(t)=\begin{cases}\dfrac{1}{\sqrt{T_c}}, & kT_s \le t < (k+1)T_s \\ 0, & \text{others}\end{cases} \tag{8}$$

As one can easily confirm, these M functions are orthogonal to each other and any SCS chip waveform $p_{\text{SCS}}(t)$ with the same T_c and M can be written as a linear combination of $\{\psi_k(t)\}$, that is

$$p_{\text{SCS}}(t)=\sum_{k=0}^{M-1}\psi_k(t)\cdot d_k \tag{9}$$

where d_k is the projection of $p_{\text{SCS}}(t)$ onto $\psi_k(t)$, i.e.

$$d_k = M\int_0^{T_c} p_{\text{SCS}}(t)\psi_k(t)dt \tag{10}$$

Therefore, each chip symbol $p_{\text{SCS}}(t)$ corresponds to a coordinate vector

$$\boldsymbol{d}=[d_0,d_1,\cdots,d_{M-1}]^{\text{T}} \tag{11}$$

in the space spanned by $\psi_k(t)$ for $k=0,1,\cdots,M-1$. To meet the energy normalization condition of the SCS chip waveform, each vector $\boldsymbol{d}$ must satisfy

$$\frac{1}{M}\|\boldsymbol{d}\|^2=\frac{1}{M}\boldsymbol{d}^{\text{T}}\boldsymbol{d}=1 \tag{12}$$

Given the spreading chip rate f_c and the vector $\boldsymbol{d}$, the chip waveform $p(t)$ is determined. Borrowing from the notation of BCS signals (Hegarty et al., 2004), we call the vector $\boldsymbol{d}$ shape vector, and use the notation $p(t; \boldsymbol{d}, f_c)$ to denote a SCS signal whose shape vector is $\boldsymbol{d}$ and the chip rate is f_c. If it is understood from context, we will omit f_c from the notation.

It can be seen that the chip waveforms employed in most of the modulations in satellite navigation such as BPSK-R, BOC with even order, and BCS are special cases of SCS waveforms. Besides, almost all the auxiliary signal chip waveforms used in SC algorithms also belong to this family. When d=1, $p(\boldsymbol{t};\boldsymbol{d})$ degenerates to the rectangular pulse, and when $\boldsymbol{d}=[1,-1,\cdots,1,-1]^{\text{T}}_{2\ell\times 1}$, $p(\boldsymbol{t};\boldsymbol{d})$ is the chip waveform of a sine phased BOC signal with the

order $M = 2\ell$. Note that in an odd order SCS signal, the chip waveform is time-varying. For example, for sin-BOC signal with $M = 3$, the shape vector of the spreading chip is $(1,-1,1)^{\mathrm{T}}$ in the time interval $t \in \left[2nT_c, (2n+1)T_c\right)$, while it is $(-1,1,-1)^{\mathrm{T}}$ in $t \in \left[(2n-1)T_c, 2nT_c\right)$. We assume that M is even hereafter.

4.3 CCF of SCS signals

All the SC techniques are based on the shapes of CCF between the received signal and the local signal. Here we consider the CCF of two SCS signals which have the same chip rate f_c, spreading sequence $\{c_i\}$, and the order M, while the chip waveform are difference.

By using (2) and (9), a SCS baseband signal can be expressed as

$$g(t;\boldsymbol{d}) = \sum_{n=-\infty}^{+\infty} \sum_{k=0}^{M-1} (-1)^{c_n} d_k \psi_k (t - nMT_s) \tag{13}$$

The CCF of two SCS signals is

$$\begin{aligned} R_{gg'}(\tau;\boldsymbol{d},\boldsymbol{d}') &= \frac{1}{T}\int_0^T g(t)\, g'(t+\tau)\, dt \\ &= \frac{1}{T} \sum_n \sum_m \sum_{k=0}^{M-1} \sum_{q=0}^{M-1} (-1)^{c_n + c_m} d_k d'_q \int_0^T \psi_k (t - nMT_s) \psi_q (t - mMT_s + \tau)\, dt \end{aligned} \tag{14}$$

where $T = NT_c$ is the period of the spreading sequence. The integral in (14) is nonzero only when $\psi_k (t - nMT_s)$ and $\psi_q (t - mMT_s + \tau)$ have the overlapping parts. The delay τ can be expressed as the summation of three parts $\tau = aT_c + bT_s + \varepsilon$, where a is an integer, $b = 0,1,\cdots,M-1$, and $\varepsilon \in [0, T_s)$. And after some algebraic simplifications, (14) can be rewritten as (Yao & Lu, 2011)

$$\begin{aligned} R_{gg'}(\tau) &= R_{gg'}(aT_c + bT_s + \varepsilon) \\ &= R_c(a)\left[r_b\left(1 - \frac{\varepsilon}{T_s}\right) + r_{b+1}\left(\frac{\varepsilon}{T_s}\right)\right] + R_c(a+1)\left[r_{b-M}\left(1 - \frac{\varepsilon}{T_s}\right) + r_{b-M+1}\left(\frac{\varepsilon}{T_s}\right)\right] \end{aligned} \tag{15}$$

where

$$R_c(a) \triangleq \frac{1}{N} \sum_{n=0}^{N-1} (-1)^{c_n + c_{n+a}} \tag{16}$$

and the aperiodic cross-correlation function (ACCF) of $\boldsymbol{d}$ and $\boldsymbol{d}'$ is

$$r_b(\boldsymbol{d},\boldsymbol{d}') = \begin{cases} \dfrac{1}{M} \displaystyle\sum_{i=0}^{M-1-b} d_i d'_{b+i}, & 0 \le b \le M-1 \\ \dfrac{1}{M} \displaystyle\sum_{i=0}^{M-1-b} d_{i-b} d'_i, & 1-M \le b < 0 \\ 0, & |b| \ge M \end{cases} \tag{17}$$

By using (15) one can derive other expression form of an *M*-order BOC signal ACF, which is

$$R_{\mathrm{BOC}}(\tau)=\begin{cases}(-1)^{k+1}\left[\frac{\tau(2M-2k-1)}{T_c}-\frac{2(M-1)k-2k^2+M}{M}\right], & \frac{kT_c}{M}\le\tau<\frac{(k+1)T_c}{M}\\ (-1)^{k+1}\left[\frac{\tau(2k-1)}{T_c}+\frac{(M-k)(2k-1)-k}{M}\right], & \frac{(k-M)T_c}{M}\le\tau<\frac{(k-M+1)T_c}{M}\\ 0, & \text{others}\end{cases} \tag{18}$$

where $k=0,1,\cdots,M-1$. And the CCF between an *M*-order BOC signal and a SCS signal is

$$R_{\mathrm{B/L}}(\tau;\boldsymbol{d}_L)=\begin{cases}\left(\frac{\tau M-kT_c}{T_c}\right)(r_{k+1}-r_k)+r_k, & \frac{kT_c}{M}\le\tau<\frac{(k+1)T_c}{M}\\ \left(\frac{\tau M-kT_c+MT_c}{T_c}\right)(r_{k-M+1}-r_{k-M})+r_{k-M}, & \frac{(k-M)T_c}{M}\le\tau<\frac{(k-M+1)T_c}{M}\\ 0, & \text{others}\end{cases} \tag{19}$$

where $\boldsymbol{d}_L$ is the shape vector of SCS signal, and

$$r_k=\begin{cases}\frac{1}{M}\sum_{i=0}^{M-1-k}(-1)^i d_{k+i}, & 0\le k\le M-1\\ \frac{1}{M}\sum_{i=0}^{M-1-k}(-1)^{i-k} d_i, & 1-M\le k<0\\ 0, & |k|\ge M\end{cases} \tag{20}$$

Fig. 9 shows a schematic diagram of $R_{\mathrm{B/L}}(\tau;\boldsymbol{d}_L)$. Note that within (-$T_c$,$T_c$) the correlation function is piecewise linear between kT_s and $(k+1)T_s$, and $R_{\mathrm{B/L}}(kT_s)=r_k$, for $k\in[-M+1,M-1]$ and $k\in\mathbb{Z}$.

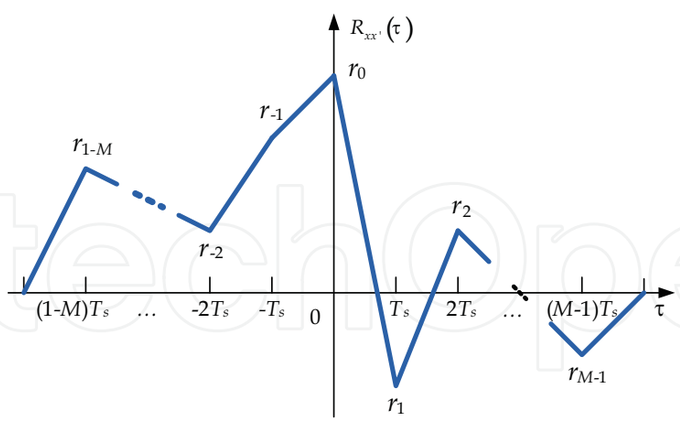

Fig. 9. Schematic diagram of correlation function $R_{\mathrm{B/L}}(\tau;\boldsymbol{d}_L)$.

4.4 SC algorithm design process under SC framework

From (15) and (17), it can be seen that the CCF of two SCS signals mostly depends on the ACCF of their chip waveforms when these two signals have the same spreading sequences. In SC algorithm design, since the chip waveform shape of the received signal is known, CCF entirely depends on the shape of local signal spreading chip waveform. Note that each SCS

chip waveform corresponds to an unique point in M-dimensional space whose coordinate is $(d_0, d_1, \cdots, d_{M-1})$, so by changing the value of d_k, one can adjust the shape of CCF. That is, CCF is a function of $\boldsymbol{d}$.

After building the relation between the shape of CCF and the value of a vector, the search for good chip waveform can be equivalent to an optimization problem which can be formulated as

$$\begin{cases} \min f(\boldsymbol{d}_1, \boldsymbol{d}_2, \cdots, \boldsymbol{d}_n); \\ s.t. \quad g_i(\boldsymbol{d}_1, \boldsymbol{d}_2, \cdots, \boldsymbol{d}_n) \geq 0, i = 1, \cdots, m \end{cases} \tag{21}$$

where f is the objective function, g_i is the constraint function, m is the number of constraints, and $\boldsymbol{d}_1, \cdots, \boldsymbol{d}_n$ are shape vectors of local signals. Then the development of SC algorithm becomes the solving of an optimization problem with a set of inequalities constraints and can be achieved through four steps (Yao & Lu, 2011), as shown in Figure 10.

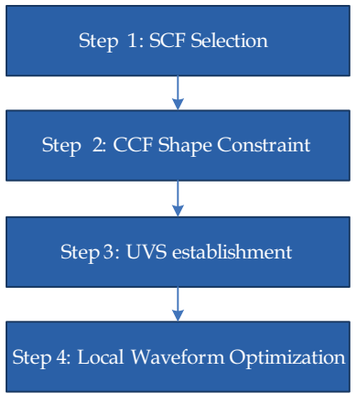

Fig. 10. SC Algorithm Design Process under SC Framework

The first step is SCF selection. In SC algorithms, the SCF $\tilde{R}$ is used instead of ACF in acquisition and tracking. The choice of SCF determines the combination mode of CCFs, and provides for the number of local auxiliary signals. The more local signals are used to form SCF, the more flexible the shape control is, but the more correlators are needed as well.

The second step is CCF shape constraint. Once the SCF is determined, the shape of each CCF employed in SCF can be restricted. Since CCF is piecewise linear between its values at integer multiples of T_c / M, and $R_{gg'}(kT_c / M) = r_k$, the constraint of the i'th CCF shape can be translated into the restriction on values of those $r_k^{(i)}$.

The third step is referred to as unambiguous vector subset (UVS) establishment. Using the corresponding relationship between $r_k^{(i)}$ and the shape vector $\boldsymbol{d}_i$ of local signal, one can further translate the restriction on the value of $r_k^{(i)}$ into the limitation of $\boldsymbol{d}_i$. In most cases, the values of each $r_k^{(i)}$ which makes the SCF unambiguous are not unique, thus the feasible solution of $\boldsymbol{d}_i$ is not a fixed point. The feasible region of $\boldsymbol{d}_i$ is denoted as $\mathcal{S}_i \subset \mathbb{R}^M$ and is called UVS of $\boldsymbol{d}_i$.

The final step is local waveform optimization. As the UVS has been established, with an optimization object, (21) can be rewritten as

$$\begin{cases} \min f\left(\boldsymbol{d}_1, \boldsymbol{d}_2, \cdots, \boldsymbol{d}_n\right); \\ s.t. \quad \boldsymbol{d}_i \in \mathcal{S}_i, i = 1, \cdots, n \end{cases} \tag{22}$$

and the final step is to find n optimal shape vectors $\boldsymbol{d}_1^{(\mathrm{opt})}$, $\boldsymbol{d}_2^{(\mathrm{opt})}$,…, $\boldsymbol{d}_n^{(\mathrm{opt})}$ from UVS, which correspond to the optimal local chip waveforms.

Note that usually at different processing stages, the optimization objects are difference. For example, in acquisition, the optimization objects may be the maximum SNR or the widest SCF main peak, while at tracking stage it may be the ability of multipath rejection, the greatest slope or the widest linear range of the discriminator curve, or even some compromises between them. In next two sections, we will give two examples of SC algorithm design under the steps described above. The design process of an SC unambiguous acquisition algorithm as well as an SC unambiguous tracking loop is described respectively.

5. GRASS technique

Under the analytic design framework described above, an unambiguous acquisition technique named General Removing Ambiguity via Side-peak Suppression (GRASS) technique is developed. This technique is suitable for generic sin-BOC(kn,n) signals and it is convenient to implement. The detailed performance analysis of this technique can be found in (Yao et al., 2010a). This section puts its emphasis on the design process of this technique.

5.1 Step 1 - SCF selection

Theoretically, when the number of local auxiliary signals is unlimited, SCF can be shaped into any desired forms. However, from the view of engineering, the more local signals are used, the more correlators are needed in a receiver which is directly related to the complexity and power consumption. Moreover, the noncoherent combination of too much correlator results may aggravate SNR deterioration. Therefore, in our design, the number of local auxiliary signals should be as few as possible.

Since the signal acquisition is a process of searching pronounced energy peak in a 2-dimentional space, the requirement to the shape of SCF in acquisition is relatively generous compared to code tracking. A SCF having main peak without positive side peak is enough. Therefore in GRASS technique only one local auxiliary SCS signal with a matched BOC signal is employed to suppress the side peaks of BOC ACF in noncoherent mode. The SCF used is as follow:

$$\tilde{R}\left(\Delta\tau\right) = R_{\mathrm{B}}^2\left(\Delta\tau\right) - \alpha R_{\mathrm{B/L}}^2\left(\Delta\tau\right) \tag{23}$$

where R_{B} is the ACF of BOC signal, $R_{\mathrm{B/L}}$ is the CCF between the received BOC signal and the local SCS signal, and α is the weight coefficient. It can be seen that (23) is similar with the SCF used in (Julien et al., 2007) in form. However, as shown later, GRASS technique is not only suitable for BOC(n,n) signals but also for other BOC$\left(kn,n\right)$ signals.

5.2 Step 2 - CCF shape constraint

The objective is to keep the main peak of BOC ACF envelop while remove all the positive side peaks (the negative side peaks do not interfere with the statistical test since only

positive values could pass the threshold). In consideration of the shape of BOC ACF, it is desirable that the envelop of $R_{\mathrm{B/L}}$ be zigzag and symmetric with respect to $\tau = 0$. Moreover, $R_{\mathrm{B/L}}^2(0)$ should be zero in order to ensure that the magnitude of main peak is unaffected after the subtracting.

As explained in the previous section, the above constraints of the CCF shape can be translated into the restriction on r_k via (19). The constraint $R_{\mathrm{B/L}}^2(0) = 0$ is equivalent to

$$r_0 = 0 \tag{24}$$

and the axial symmetry of $\left|R_{\mathrm{B/L}}\right|$ means

$$\left|r_i\right| = \left|r_{-i}\right| \tag{25}$$

The requirement of zigzag shape can be realized through making adjacent r_k have opposite sign, that is

$$\begin{cases} r_i r_{i+1} < 0, & i > 0 \\ r_i r_{i-1} < 0, & i < 0 \end{cases} \tag{26}$$

Actually, under the restrictions of (24) and (26), (25) can be simplified to

$$r_i = -r_{-i} \tag{27}$$

because by (20) and (24) we have

$$\begin{aligned} \left|r_{M/2} + r_{-M/2}\right| &= \frac{1}{M}\left|\sum_{i=0}^{M/2-1}(-1)^i d_{i+M/2} + \sum_{i=0}^{M/2-1}(-1)^{i-M/2} d_i\right| \\ &= \frac{1}{M}\left|\left(\sum_{i=0}^{M/2-1} + \sum_{i=M/2}^{M-1}\right)(-1)^{i-M/2} d_i\right| \\ &= \frac{1}{M}\left|\sum_{i=0}^{M-1}(-1)^i d_i\right| = \left|r_0\right| = 0 \end{aligned} \tag{28}$$

so that $r_{M/2} = -r_{-M/2}$. Then using (26), we obtain (27).

5.3 Step 3 - UVS establishment

Substituting (20) into (24), (26) and (27), after some straightforward algebraic simplification, we have the set of inequalities constraints on the elements of $\boldsymbol{d}_L$:

$$\begin{cases} \sum_{i=0}^{k}(-1)^i d_i > 0, & k = 0,1,\cdots,\frac{M}{2}-1 \\ d_k = d_{M-1-k}, & k = 0,1,\cdots,\frac{M}{2}-1 \\ \sum_{i=0}^{M-1} d_i^2 = M \end{cases} \tag{29}$$

Note that the last term in (29) is the energy normalization constraint of SCS waveform. So that the UVS can be represented as

$$\mathcal{S}=\left\{\begin{array}{c}\sum_{i=0}^{M-1}d_i^2=M\\ \boldsymbol{d}_L\in\mathbb{R}^M:\sum_{i=0}^{k}(-1)^i d_i>0\\ d_k=d_{M-1-k},k=0,1,\cdots,\frac{M}{2}-1\end{array}\right\} \tag{30}$$

With an appropriate weight coefficient α, all the undesired positive side peaks of R_{B}^2 can be canceled by subtraction. From (18), the coefficient α must satisfies

$$\alpha|r_k|\geq\left|R_B\left(kT_c/M\right)\right|=\frac{M-k}{M} \tag{31}$$

for $k=1,2,\cdots,M-1$, or

$$\alpha\geq\max_{k\neq0}\frac{M-k}{M|r_k|}. \tag{32}$$

5.4 Step 4 - Local waveform optimization

So far the effect of thermal noise has not been considered. In fact, the coefficient α amplifies noise components in $R_{\mathrm{B/L}}$. Under a given pre-correlation SNR, the larger α is, the lower SNR in the SCF is. Therefore, from the viewpoint of sensitivity, it is desired that α be as small as possible. So that with a given $\boldsymbol{d}_L$ the optimum α is

$$\alpha=\max_{k\neq0}\frac{M-k}{M\left|r_k\left(\boldsymbol{d}_L\right)\right|} \tag{33}$$

and in UVS, the optimum $\boldsymbol{d}_L$ is the one minimizing α, that is

$$\boldsymbol{d}_{\mathrm{opt}}=\arg\min_{\boldsymbol{d}_L\in\mathcal{S}}\alpha=\arg\min_{\boldsymbol{d}_L\in\mathcal{S}}\max_{k\neq0}\frac{M-k}{M|r_k|} \tag{34}$$

It can be proved that the explicit expression of (34) is

$$\boldsymbol{d}_{\mathrm{opt}}=\left[d_0,d_1,\cdots d_{M-1}\right]^{\mathrm{T}} \tag{35}$$

where

$$\begin{cases}d_0=d_{M-1}=\frac{M-1}{\sqrt{2M-3}}\\ d_i=d_{M-i+1}=\frac{(-1)^{i-1}}{\sqrt{2M-3}},\left(i=1,2,\cdots,\frac{M}{2}-1\right)\end{cases} \tag{36}$$

and $\alpha_{\min}=2M-3$.

Figure 11 (a)-(c) depict the optimum local SCS waveforms for BOC(n,n), BOC(2n,n), and BOC(3n,n) signals respectively. For BOC(n,n) signals, $M=2$. So $\boldsymbol{d}_{\mathrm{opt}}=(1,1)^{\mathrm{T}}$ and $\alpha_{\min}=1$. It can be found that the SC method proposed in (Julien, et al., 2007) is equivalent to this case. The local symbol is simply a rectangular pulse. For BOC(2n,n), $\boldsymbol{d}_{\mathrm{opt}}=\sqrt{\frac{9}{5}}\left(1,\frac{1}{3},\frac{1}{3},1\right)^{\mathrm{T}}$ and $\alpha_{\min}=5$. For BOC(3n,n), $\boldsymbol{d}_{\mathrm{opt}}=\frac{1}{3}(5,1,-1,-1,1,5)^{\mathrm{T}}$ and $\alpha_{\min}=9$. It can be seen that the

complexity of the chip shape increases as the BOC-modulation order is raised. For $M = 4$ or higher, the optimum local SCS waveform is hard to obtain by geometrical intuition. Figure 12, 13, and 14 show the envelop of R_B, $R_{B/L}$ and the SCF for $M = 2$, 4, 6, respectively.

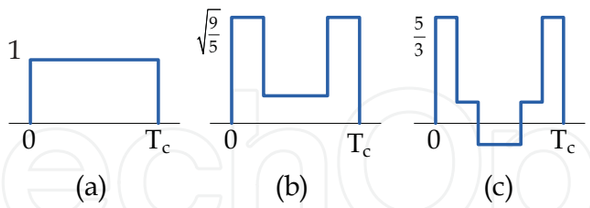

Fig. 11. Optimum Local SCS Waveforms for (a) M=2, (b) M=4, (c) M=6

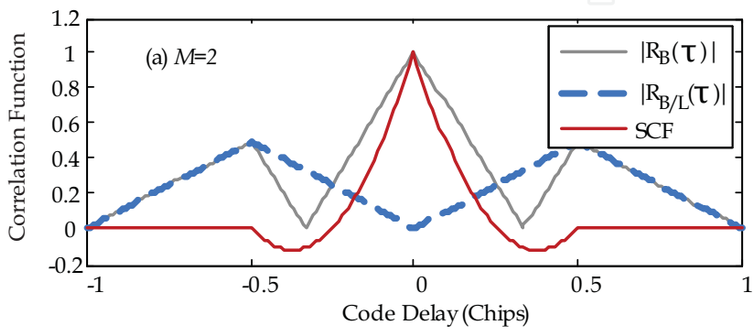

Fig. 12. The Envelops of R_B, $R_{B/L}$ and the SCF for M=2

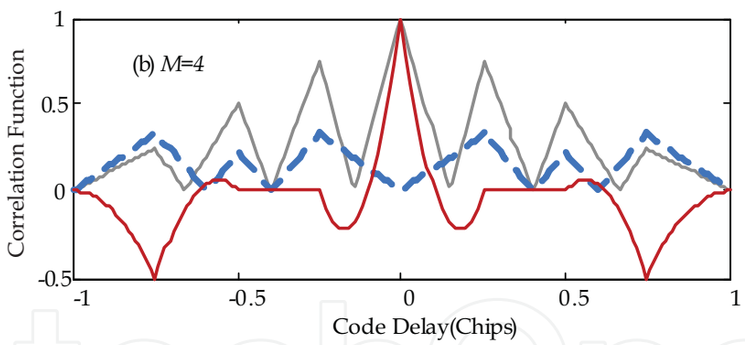

Fig. 13. The Envelops of R_B, $R_{B/L}$ and the SCF for M=4

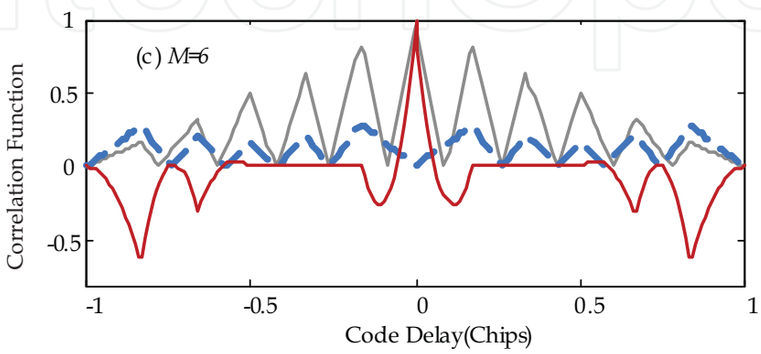

Fig. 14. The Envelops of R_B, $R_{B/L}$ and the SCF for M=6

From the figures it can be seen that with any *M*, no major positive side peak exists in SCF. Although there are some pits on the SCF, their magnitudes are all below zero, so they bring no threat to the acquisition.

Although all examples shown above are for sin-BOC signals, it is easy to demonstrate that GRASS technique can also be applied to cos-BOC signals by simply replacing basis function (8) with

$$\psi_k'(t)=\begin{cases}\dfrac{1}{\sqrt{T_c}}\operatorname{sgn}\left\{\sin\left[2\pi f_s\left(t-kT_s\right)\right]\right\}, & kT_s\le t<\left(k+1\right)T_s\\ 0, & \text{others}\end{cases} \tag{37}$$

6. PUDLL

As another example of the application of SC design framework, in this section we show the design process of an unambiguous code tracking technique named pseudo-correlation-function-based unambiguous delay lock loop (PUDLL) (Yao et al., 2010b) which is applicable to any BOC(*kn*,*n*) signals. At tracking stage, because the discriminator characteristic curve is based on the first derivative of SCF, the requirement to the shape of SCF is more stringent than in acquisition.

6.1 Step 1 – SCF selection

It is desired that the SCF used in code tracking has an ideal triangular main peak with no side peak. Since the CCF between the received BOC signal and the local SCS signal is piecewise linear, utilizing this characteristic, and using the absolute-magnitude operation to change the direction of lines on one side of the zero crossing point, following by the linear combination, it is possible to obtain the SCF without any side peak. Therefore, in this example, the SCF is chosen as

$$\tilde{R}(\tau)=\left|R_1(\tau)\right|+\left|R_2(\tau)\right|-\left|R_1(\tau)+R_2(\tau)\right| \tag{38}$$

where R_1 and R_2 are CCFs between BOC signal and two local SCS signals $g_1(t;\boldsymbol{d}_1)$ and $g_2(t;\boldsymbol{d}_2)$, respectively, in which $\boldsymbol{d}_1$ and $\boldsymbol{d}_2$ are the shape vectors of g_1 and g_2 respectively.

6.2 Step 2 – CCF shape constraint

A sufficient condition for (38) being symmetric with respect to $\tau=0$ is

$$\left|R_1(\tau)\right|=\left|R_2(-\tau)\right|. \tag{39}$$

In fact, the only difference between $R_1(\tau)=R_2(-\tau)$ and $R_1(\tau)=-R_2(-\tau)$ lies in the polarity of the local SCS chip waveform. Without loss of generality, assume $R_1(\tau)=-R_2(-\tau)$, so that at each endpoint of CCF segment

$$r_i'=-r_i \tag{40}$$

where $r_i=R_1(iT_c/M)$ and $r_i'=R_2(iT_c/M)$.

From (38), it can be proved that $\tilde{R}$ is also piecewise linear. In order to shape the SCF into an ideal triangle, one have to make all of the ending points of lines in $\tilde{R}$ be zero except the central one.

To ensure the triangular shape, SCF must satisfy the following request:

$$\begin{cases} \tilde{R}(0) \neq 0 \\ \tilde{R}(kT_c / M) = 0, (k \neq 0) \end{cases} \tag{41}$$

where the first term is equivalent to

$$r_0 = 0 \tag{42}$$

and using (38) and (40), the second term can be simplified as

$$r_k r_{-k} \leq 0 \tag{43}$$

for $k \neq 0$.

The constraints (42) and (43) are necessary but not sufficient, since the absolute-magnitude operation introduces additional endpoints at the zero crossing points in R_1 and R_2. If R_1 has a zero crossing point τ_0 within the interval $\left[kT_c / M, (k+1)T_c / M\right]$, $(k > 0)$, easily proved, it must be

$$\tau_0 = \frac{kT_c}{M} + \frac{|r_k|}{|r_k| + |r_{k+1}|} \frac{T_c}{M} \tag{44}$$

From (43) we know that R_2 must have a zero crossing point within the same interval, which is

$$\tau_0' = \frac{kT_c}{M} + \frac{|r_{-k}|}{|r_{-k}| + |r_{-k-1}|} \frac{T_c}{M} \tag{45}$$

In order to eliminate the inclined lines on both sides of the zero crossing point, we must have $\tau_0 = \tau_0'$, which can be simplified as

$$r_k r_{-k-1} = r_{-k} r_{k+1} \tag{46}$$

for $k > 0$.

6.3 Step 3 – UVS establishment

The necessary and sufficient conditions for SCF being triangular are (40), (42), (43), and (46). From (40), we obtain that $\boldsymbol{d}_1$ and $\boldsymbol{d}_2$ are mirror images of each other, i.e.

$$d_k' = d_{M-k-1} \tag{47}$$

where d_k and d_k' are the entries of $\boldsymbol{d}_1$ and $\boldsymbol{d}_2$, respectively. When $M = 2$, by using the relationship (20), the UVS can be represented as

$$\mathcal{S} = \left\{ \boldsymbol{d}_1 \in \mathbb{R}^2 : d_1^2 + d_2^2 = 2, d_0 > d_1 \geq 0 \right\} \tag{48}$$

In the case $M = 4$ (Yao, 2008), UVS can be expressed as

$$\mathcal{S} = \left\{ \boldsymbol{d}_1 \in \mathbb{R}^4 \left| \left\{ \begin{array}{c} d_0 > d_3 \geq 0 \\ d_1 = d_2 = 0 \end{array} \right\} \bigcup \left\{ \begin{array}{c} 0 \leq d_3 \leq d_0 \leq d_1 \\ d_3 \leq d_2 \\ -d_3 \leq d_1 - d_2 \leq d_0 \\ d_0 - d_1 + d_2 - d_3 \neq 0 \end{array} \right\} \right. \right\} \tag{49}$$

For larger M, as the degrees of freedom of $\boldsymbol{d}_1$ increase, the explicit expressions for the constraints on $\boldsymbol{d}_1$ become complex and hard to derive. The full UVS can be obtained through the use of numerical method. However, it is easy to verify that any element in one of the subset of UVS

$$\mathcal{S}' = \left\{ \boldsymbol{d}_1 \in \mathbb{R}^M \left| \left\{ \begin{array}{l} d_0 > d_{M-1} \geq 0 \\ d_i = 0, i = 1, 2, \cdots, M-2 \end{array} \right\} \right. \right\} \tag{50}$$

can make a triangular SCF for all M even.

6.4 Step 4 – Local waveform optimization

Under the energy normalization restriction (12), $\boldsymbol{d}_1$ in (50) has one degree of freedom. So by defining $\kappa = d_{M-1} / d_0$, the shape vector in $\mathcal{S}'$ can be expressed as

$$\boldsymbol{d}_1 = \left(\sqrt{\tfrac{M}{1+\kappa^2}}, 0, \cdots, 0, \kappa \sqrt{\tfrac{M}{1+\kappa^2}} \right)^{\mathrm{T}} \tag{51}$$

Utilizing (51), (19), and (38), without considering front-end filtering, we can obtain the expression of $\tilde{R}$

$$\tilde{R}(\tau;\kappa) = \begin{cases} \frac{M(2\kappa-4)|\tau| + 2(1-\kappa)T_c}{\sqrt{M(1+\kappa^2)}T_c}, & |\tau| < \frac{(1-\kappa)T_c}{M(2-\kappa)} \\ 0, & \text{others} \end{cases} \tag{52}$$

the base line half width of which is

$$w(\kappa) = \frac{(1-\kappa)T_c}{M(2-\kappa)} \tag{53}$$

and the height of the peak is

$$h(\kappa) = \frac{2(1-\kappa)}{\sqrt{M(1+\kappa^2)}} \tag{54}$$

Figure 15 (a) and (b) show some SCFs with different κ for BOC(n,n) and BOC(2n,n) signals, respectively. Figure 16 depicts the discriminator characteristic curve of the early-minus-late power (EMLP) loop which uses SCF instead of BOC(n,n) ACF.

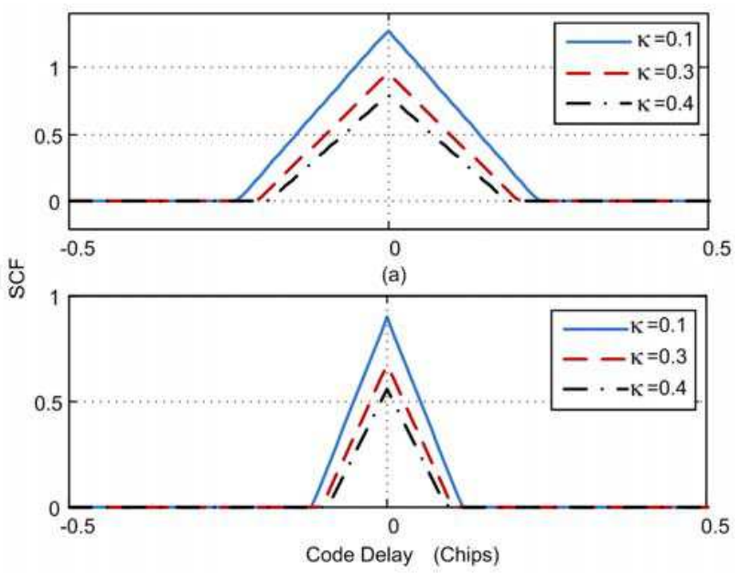

Fig. 15. SCF for (a) BOC(*n*,*n*) and (b) BOC(2*n*,*n*) Signals, with Different κ

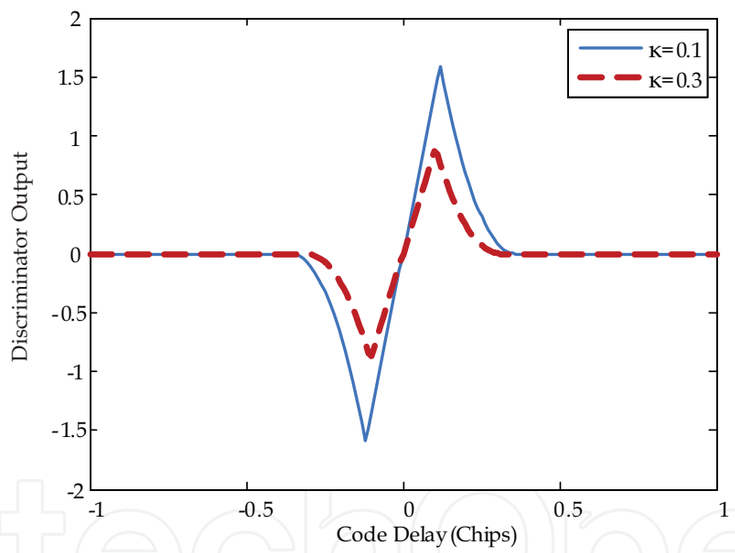

Fig. 16. The Discriminator Characteristic Curve for BOC(*n*,*n*) Signals, with Different κ

It can be noted that by using SCF, this technique completely removes the false lock points. And it can also be seen that both shapes of SCF and discriminator characteristic curve are functions of κ. Consequently, changing the value of κ can adjust the linear range of the discriminator and the slope of the curve, thus changes the multipath and thermal noise mitigation performances of the tracking loop (Yao, Cui, et al., 2010). With different optimization objective, the optimum κ and the optimum chip waveform are not the same.

7. Conclusion

In this Chapter, the ambiguity problem of BOC modulated signals which have been chosen as the chief candidate for several navigation signals in the next generation GNSS as well as

its solutions is systematically described. An innovative design methodology for future unambiguous processing techniques is also proposed. Under the proposed design framework, the development of SC algorithm becomes the solving of an optimization problem with a set of inequalities constraints and can be achieved through four steps.

As two practical examples, the design process of an SC unambiguous acquisition algorithm as well as an SC unambiguous tracking loop is described respectively to demonstrate the practicality of the proposed framework and to provide reference to further SC algorithm development. Although the optimization objects are difference in these two algorithms, the methods of analysis and the design steps under the analytic design framework are unified. It is proved that both of these two algorithms can completely eliminate the ambiguity problem in acquisition and tracking. Moreover, these two algorithms have outstanding compatibility. Both of them are suitable for generic even-order sine-BOC signal.

Future works will focus on the development of new algorithms under the proposed framework. Considering the complexities, both of the example algorithms in this Charpter employ only two local signals. In fact, by using more local signals, degrees of freedom in design can be further increased and the shape control will be more flexible. Besides, this analytic design framework can be used not only on unambiguous algorithm development but also on finding good local waveform to resist the effect of multipath.

8. References

ARINC. (2005). NAVSTAR GPS space segment/navigation L5 User interfaces. In *IS-GPS-705*.

ARINC. (2006). Navstar GPS space segment/user L1C interfaces. In *IS-GPS-800*. El Segundo, CA, US.

Avila-Rodriguez, J.-A., Hein, G. W., Wallner, S., Issler, J.-L., Ries, L., Lestarquit, L., Latour, A. d., Godet, J., Bastide, F., Pratt, T., & Owen, J. (2007). The MBOC modulation: the final touch to the Galileo frequency and signal plan, *Proceedings of ION GNSS 20th International Technical Meeting of the Satellite Division*, pp. 1515-1529, Fort Worth, TX, US, 2007.

Betz, J. W. (2001). Binary offset carrier modulations for radionavigation, *Navigation: J. Inst. Navig.*, 48(4), 227-246.

Burian, A., Lohan, E. S., & Renfors, M. (2006). BPSK-like methods for hybrid-search acquisition of Galileo signals, *Proceedings of IEEE ICC 2006*, pp. 5211-5216, Istanbul, Turkey, 2006.

Dovis, F., Mulassano, P., & Presti, L. L. (2005). A novel algorithm for the code tracking of BOC(*n*,*n*) modulated signals, *Proceedings of ION GNSS 2005*, pp. 152-155, Long Beach, CA, 2005.

Enge, P. (2003). GPS modernization: capabilities of the new civil signals. *Proceedings of Australian International Aerospace Congress*, pp. 1-22. Brisbane, 2003.

Fante, R. L. (2003). Unambiguous tracker for GPS binary-offset-carrier signals, *Proceedings of the 59th Annual Meeting of The Institute of Navigation and CIGTF 22nd Guidance Test Symposium*, pp. 141-145, Albuquerque, NM, US, 2003.

Fine, P., & Wilson, W. (1999). Tracking algorithm for GPS offset carrier signals. *Proceedings of ION NTM 1999*, pp. 671-676, San Diego, CA, US, 1999.

Fishman, P., & Betz, J. W. (2000). Predicting performance of direct acquisition for the M-code signal. *Proceedings of ION NTM 2000*, pp. 574-582, Anaheim, CA, US, 2000.

Gao, G. X., Chen, A., Lo, S., Lorenzo, D. d., & Enge, P. (2007). GNSS over China - the Compass MEO satellite codes. *Inside GNSS,* 2007, 2(5), pp. 36-43.

Hegarty, C. J., Betz, J. W., & Saidi, A. (2004). Binary coded symbol modulations for GNSS. *Proceedings of ION 60th Annual Meeting*, pp. 56-64, Dayton, OH, US, 2004.

Hegarty, C. J., & Chatre, E. (2008). Evolution of the global navigation satellite system (GNSS). *Proceedings of IEEE,* 96(12), pp. 1902-1917.

Hein, G. W., Avila-Rodriguez, J.-A., Wallner, S., Pratt, A. R., Owen, J., Issler, J.-L., Betz, J. W., Hegarty, C. J., Lenahan, L. S., Rushanan, J. J., Kraay, A. L., & Stansell, T. A. (2006). MBOC: the new optimized spreading modulation recommended for GALILEO L1 OS and GPS L1C. *Proceedings of IEEE/ION PLANS 2006*, pp. 883-892, San Diego, CA, US, 2006.

Julien, O., Macabiau, C., Cannon, M. E., & Lachapelle, G. (2007). ASPeCT: unambiguous sine-BOC(n,n) acquisition/tracking technique for navigation applications, *IEEE Transactions on Aerospace and Electronic Systems,*Vol. 43, No.1, pp. 150-162.

Lohan, E. S., Burian, A., & Renfors, M. (2008). Low-complexity unambiguous acquisition methods for BOC-modulated CDMA signals, *Int. J. Commun. Syst. Network,* 26 (2008), pp. 503–522.

Martin, N., Leblond, V., Guillotel, G., & Heiries, V. (2003). BOC(x,y) signal acquisition techniques and performances. *Proceedings of ION GPS 2003*, pp. 188-198, Portland, OR, US, 2003.

Musso, M., Cattoni, A. F., & Regazzoni, C. S. (2006). A new fine tracking algorithm for binary offset carrier modulated signals. *Proceedings of ION GNSS 2006*, pp. 834-840, Fort Worth, TX, US, 2006.

Nunes, F., Sousa, F., & Leitao, J. (2007). Gating functions for multipath mitigation in GNSS BOC signals, *IEEE Transactions on Aerospace and Electronic Systems,* Vol. 43, No. 3 (2007), pp. 941-964.

Proakis, J. G. (2001). *Digital Communications*, Boston: McGraw-Hill Companies, Inc.

Slater, J. A., Weber, R., & Fragner, E. (2004). The IGS GLONASS pilot project – transitioning an experiment into an operational GNSS service. *Proceedings of ION GNSS 2004*, pp. 1749 – 1757, Long Beach, CA, US, 2004.

VanDierendonck, A. J., Fenton, P., & Ford, T. (1992). Theory and performance of narrow correlator spacing in GPS receiver, *Navigation: J. Inst. Navig.,* Vol. 39, pp. 115 - 124.

Ward, P. W. (2003). A design technique to remove the correlation ambiguity in binary offset carrier (BOC) spread spectrum signals. *Proceedings of ION AM 2003*, pp. 146-155, Albuquerque, NM, US, 2003.

Yao, Z. (2008). A new unambiguous tracking technique for sine-BOC(2*n*,*n*) signals. *Proceedings of ION GNSS 2008,* pp. 1490-1496, Savannah, GA, US, 2008.

Yao, Z. (2009). *Code Synchronization and Carrier Tracking Algorithms for New Generation of GNSS.* PhD Thesis, Tsinghua University, Beijing.

Yao, Z., Cui, X., Lu, M., & Feng, Z. (2010b). Pseudo-correlation-function-based unambiguous tracking technique for sine-BOC signals. *IEEE Transactions on Aerospace and Electronic Systems,* Vol. 46, No. 4, pp. 1782-1796.

Yao, Z., & Lu, M. (2011). Side-peaks cancellation analytic design framework with applications in BOC signals unambiguous processing, *Proceedings of ION ITM 2011*, pp. 775-785, San Diego, CA, US, 2011.

Yao, Z., Lu, M., & Feng, Z. (2010a). Unambiguous sine-phased binary offset carrier modulated signal acquisition technique, *IEEE Transactions on Wireless Communications,* Vol. 9, No. 2, pp. 577-580.

Ziemer, R. E., & Peterson, R. L. (1985). *Digitial Communications and Spread Spectrum Systems*. New York: Macmillan Publishing Company.

Global Navigation Satellite Systems: Signal, Theory and Applications

Edited by Prof. Shuanggen Jin

ISBN 978-953-307-843-4
Hard cover, 426 pages
Publisher InTech
Published online 03, February, 2012
Published in print edition February, 2012

Global Navigation Satellite System (GNSS) plays a key role in high precision navigation, positioning, timing, and scientific questions related to precise positioning. This is a highly precise, continuous, all-weather, and real-time technique. The book is devoted to presenting recent results and developments in GNSS theory, system, signal, receiver, method, and errors sources, such as multipath effects and atmospheric delays. Furthermore, varied GNSS applications are demonstrated and evaluated in hybrid positioning, multi-sensor integration, height system, Network Real Time Kinematic (NRTK), wheeled robots, and status and engineering surveying. This book provides a good reference for GNSS designers, engineers, and scientists, as well as the user market.

InTech Europe
University Campus STeP Ri
Slavka Krautzeka 83/A
51000 Rijeka, Croatia
Phone: +385 (51) 770 447
Fax: +385 (51) 686 166
www.intechopen.com

InTech China
Unit 405, Office Block, Hotel Equatorial Shanghai
No.65, Yan An Road (West), Shanghai, 200040, China
中国上海市延安西路65号上海国际贵都大饭店办公楼405单元
Phone: +86-21-62489820
Fax: +86-21-62489821

IntechOpen